Zitierweise: *Angew. Chem. Int. Ed.* **2022,** *61,* e202213162
Internationale Ausgabe: doi.org/10.1002/anie.202213162
Deutsche Ausgabe: doi.org/10.1002/ange.202213162

Photocatalytic CO_2 Reduction

Complexed Semiconductor Cores Activate Hexaniobate Ligands as Nucleophilic Sites for Solar-Light Reduction of CO_2 by Water

*Guanyun Zhang, Fei Wang, Tal Tubul, Mark Baranov, Nitai Leffler, Alevtina Neyman, Josep M. Poblet, and Ira A. Weinstock**

Abstract: Although pure and functionalized solid-state polyniobates such as layered perovskites and niobate nanosheets are photocatalysts for renewable-energy processes, analogous reactions by *molecular* polyoxoniobate cluster-anions are nearly absent from the literature. We now report that under simulated solar light, hexaniobate cluster-anion encapsulated 30-Ni^{II}-ion "fragments" of surface-protonated cubic-phase-like NiO cores activate the hexaniobate ligands towards CO_2 reduction by water. Photoexcitation of the NiO cores promotes charge-transfer reduction of Nb^{V} to Nb^{IV}, increasing electron density at bridging oxo atoms of Nb-μ-O-Nb linkages that bind and convert CO_2 to CO. Photogenerated NiO "holes" simultaneously oxidize water to dioxygen. The findings point to molecular complexation of suitable semiconductor "fragments" as a general method for utilizing electron-dense polyoxoniobate anions as nucleophilic photocatalysts for solar-light driven activation and reduction of small molecules.

Solid-state polyniobates[1] such as the layered perovskite, $K_4Nb_6O_{17}$,[2] calcium-niobate nanosheets, $KCa_2Nb_3O_{10}$,[3] and binary oxides such as $SrNb_2O_6$,[4] are photocatalysts for water oxidation, H_2 evolution and CO_2[5] reduction, with activities enhanced by interactions with incorporated metal[3b,c,6] or metal-oxide[2b,3d,7] nanoparticles. By contrast, photocatalysis by *molecular* polyoxoniobate cluster-anions[8] is nearly absent from the literature.

One reason is that the excitation of electrons from the highest-occupied to lowest-unoccupied molecular orbitals, i.e. HOMOs to LUMOs, within the molecular clusters requires ca. 5 eV (250 nm),[9] versus the ca. 3.5 eV (354 nm) band gaps that allow for solar-light driven catalysis by solid-state niobates.[1] Notably, however, the O atoms of bridging Nb^{V}-μ-O-Nb^{V} linkages in polyoxoniobate clusters are highly electron dense, more so than in analogous linkages in W^{VI}- or Mo^{VI}-based cluster-anions.[10] And, electron density at bridging O atoms should increase considerably if adjacent Nb^{V} atoms were reduced to Nb^{IV}. This combination of highly energetic electrons in Nb^{IV} atoms bound to nucleophilic O atoms presents a promising scenario for binding and reducing CO_2. The challenge is to reach this attractive state using the solar spectrum.

One idea is to use hexaniobate clusters to "trap" molecular fragments of metal-oxide semiconductors whose photoexcitation can populate the ligating cluster-anion's Nb^{V}-based LUMO. In this regard, we recently used hexaniobate anions to complex metal-oxide fragments closely resembling the phase and catalytic properties of parent bulk materials.[11] For this, base-stable plenary polyoxoniobate anions combine large charge densities[12] with high symmetries that enable them to serve as *non-templating* donor ligands[12,13] that allow encapsulated metal-oxide clusters[14] to retain the phases of related bulk oxides.[11,15]

We now report that at pH values and temperatures suited to formation of cubic-NiO NCs, plenary hexaniobate anions indeed trap fragments of surface-protonated cubic-phase NiO (**1**; Figure 1A). Experimental and DFT results show that solar-light irradiation of their NiO core results in the reduction of Nb^{V} to Nb^{IV} (Figure 1B), leading to CO_2 reduction by "photo-activated" hexaniobate ligands, while NiO "holes" oxidize water[16] to O_2.

Molecular complex **1** was prepared by adding $NiCl_2$ to a basic solution of hexaniobate, ($[Nb_6O_{19}]^{8-}$, K^+ salt) and heating at 170 °C to give a blue-green solution. After work up, green, rod-like crystals of **1** were isolated at an unoptimized yield of 1.5 % (Figure S4–S7), along with colloidal NiO by-products.

Single-crystal X-ray diffraction analysis[18] of **1** revealed 30 Ni atoms encapsulated by 10 plenary-hexaniobate ligands (Figure 2; Table S1–S3) giving the highest-nuclearity nickel cluster with entirely inorganic ligands. All Ni atoms are

[*] Dr. G. Zhang, T. Tubul, M. Baranov, N. Leffler, Dr. A. Neyman, Prof. I. A. Weinstock
Department of Chemistry and the Ilse Katz Institute for Nanoscale Science & Technology, Ben-Gurion University of the Negev
Beer Sheva, 84105 (Israel)
E-mail: iraw@bgu.ac.il
Dr. G. Zhang
Key Lab for Colloid and Interface Science of Ministry of Education, School of Chemistry and Chemical Engineering
Shandong University
Jinan, 250100 (China)
Dr. F. Wang, Prof. J. M. Poblet
Departament de Química Física i Inorgànica
Universitat Rovira i Virgili
43007 Tarragona (Spain)

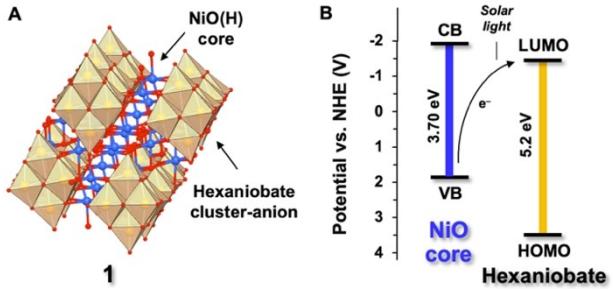

Figure 1. A) Complex, **1**, obtained by hexaniobate-anion encapsulation of a 30-Ni ion cluster. B) Solar light promotes electron transfer from the Ni^{II}-based HOMO of the NiO core to the Nb^{V}-based LUMO of ligating hexaniobate ligands. The band structure of NiO is from the literature[17] and Mott–Schottky analysis of 20-nm cubic NiO NCs (Figure S1–3); Molecular orbital (MO) energies of hexaniobate are from literature values and DFT calculations discussed below.

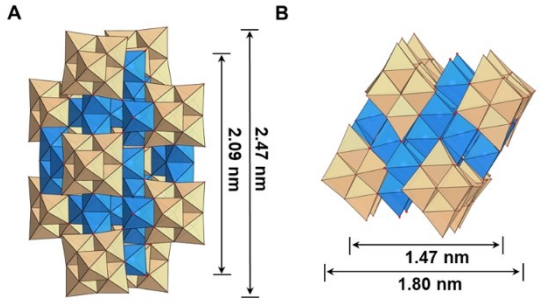

Figure 2. Polyhedral representations of **1** along the a-axis (A) and b-axis (B) and their respective dimensions in height and width. Hexaniobate ligands are in light brown; blue polyhedra contain Ni^{II} atoms.

located in pseudo-octahedral environments and linked via O atoms to give a $\{Ni_{30}O_{118}\}$ structure. The height and width of $\{Ni_{30}O_{118}\}$ are 2.09 and 1.47 nm, respectively, with inclusion of the hexaniobate ligands giving dimensions of 2.47 × 1.80 nm for **1** itself (Figure 2).

The $\{Ni_{30}O_{118}\}$ structure (Figure S8A) contains a central {Ni20} core, linked by an additional 12 μ_4-O atoms to 10 surrounding Ni atoms. Due to its small size, O atoms of 6 Ni-μ_2-O-Ni linkages and 18 Ni_3-μ_3-O linkages of the {Ni20} core are monoprotonated in water, while eight outer Ni atoms of $\{Ni_{30}O_{118}\}$ are ligated by OH_2 (bond valence sum calculations; Table S4–5). Also, 86 O atoms of $\{Ni_{30}O_{118}\}$ are supplied by 22 Nb=O and 64 Nb-μ_2-O-Nb moities of the 10 hexaniobate ligands.

The crystallographic data formulate **1** as $K_{44}[Ni_{30}(OH)_{24}(H_2O)_8(Nb_6O_{19})_{10}]\cdot 100\,H_2O$, consistent with elemental analysis and thermogravimetric analysis (Figure S9). Notably, the central $\{Ni_{30}O_{118}\}$ cluster is remarkably similar to cubic NiO (Figure S8B),[19] with protonation of surface-oxygen atoms an inherent consequence of the relatively small size of the {Ni30} fragment.

Two sets of peaks in the X-ray photoelectron spectrum of **1** (Figure S10): Ni $2p_{3/2}$ and Ni $2p_{1/2}$ at 855.2 and 873.1 eV, respectively, with broad satellite peaks, are similar to cubic NiO and $Ni(OH)_2$.[20] Temperature-dependent electron paramagnetic resonance (EPR) spectra of **1** are consistent with paramagnetic Ni^{II} ions ($3d^8$, $S=1$) in pseudo-O_h sites. At 40 K, the EPR spectrum reveals a broad asymmetric signal, centered at $g=2.08\pm0.03$ (black curve in Figure S11A), consistent with those of Ni^{II} ions in bulk NiO and $Ni(OH)_2$ ($g\approx2$).[21] Upon warming to 260 K, signal intensities obey the Curie–Weiss law, with little change in g-factor and linewidth. The EPR-estimated Weiss constant of −12 K (Figure S11B) indicated weak anti-ferromagnetic Ni^{II}-Ni^{II} interactions as reported for small NiO NCs.[22]

Tauc plots gave a 3.60 eV difference between HOMO and LUMO energies of **1** (Figure 3A). Flat-band potentials were determined by Mott–Schottky analysis. For molecular compounds, flat-band potentials are close to HOMO or LUMO energies.[23] From the negative slopes in Figure 3B, **1** exhibits p-type behavior, with a HOMO energy of 1.69 V. This, along with a 3.60 eV HOMO–LUMO gap, gives a LUMO energy of −1.91 V.

DFT calculations (see the Supporting Information for methods and references) were performed to better understand the electronic structure of **1**. Initially, two simplified models of **1**, involved 3 Ni^{II} or 7 Ni^{II} ions encapsulated by hexaniobate ligands. Calculations, performed at the PBE level, nicely reproduced the experimental geometry (Figure 4A and S12).

A more localized set of frontier MOs was obtained by single-point calculation with the hybrid B3LYP functional and the PBE optimized structure (Figure 4A). The HOMO (ca. −4 eV) is mainly localized on Ni^{II} centers, while the LUMO is localized on Nb^{V} centers. Charge migration from Ni to Nb was confirmed by in situ X-ray photoelectron spectroscopy (Figure S13), and consistent with a long fluorescence lifetime of 3.22 ns (by time-resolved photoluminescence spectroscopy; Figure S14–15). The calculated HOMO–LUMO gap of 3.70 eV is close to the experimental value of 3.60 eV (see also Figure S12). A similar experimental value of 3.3 eV was found for NiO-intercalated $K_4Nb_6O_{17}$.[24] In summary, DFT calculations show that the electronic structure (HOMO and LUMO) of **1** is comprised of NiO and hexaniobate ligands, analogous to the situation in metal- or metal-oxide intercalated niobate nanosheets.[2b,3d,25]

The experimentally determined energy levels (Figure 4B) show that the HOMO and LUMO of **1** are suitable for solar-light driven reduction of CO_2 by water. Also, the

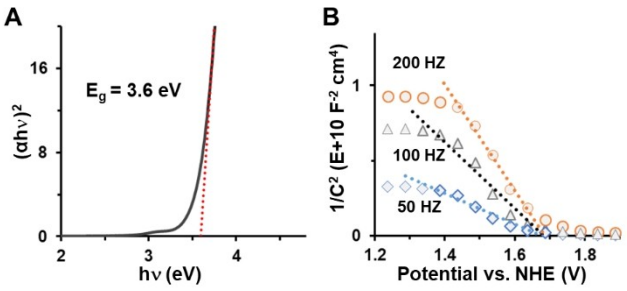

Figure 3. A) and B) Tauc and Mott–Schottky plots of **1**.

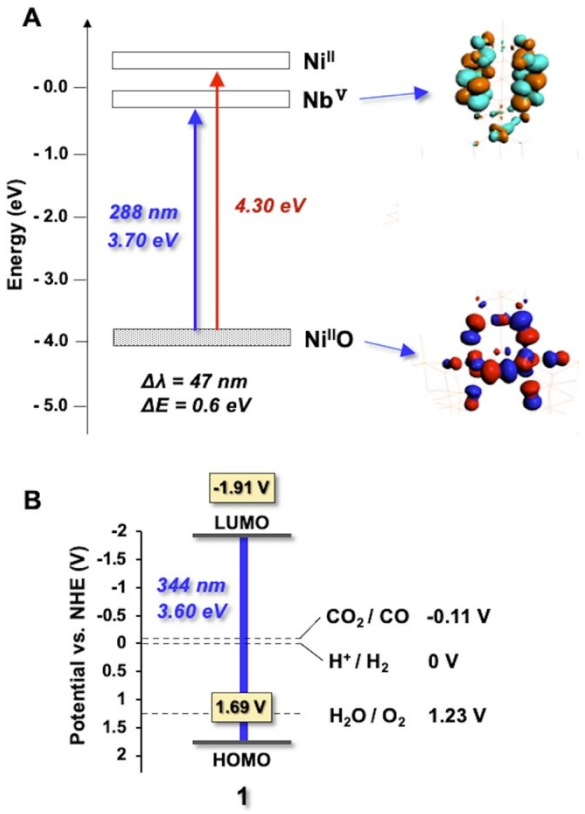

Figure 4. A) MO diagram for a simplified model $[Ni_3(OH)_4(Nb_6O_{19})_3]^{22-}$ of compound **1**. Energies of pseudo-bands for occupied and unoccupied MOs are represented by filled and empty boxes. $Ni^{II}O$, Nb^V and Ni^{II} are used to represent which atoms contribute most to each set of MOs. At right: Representative MOs. B) Energy-level diagram of **1** from data in Figure 3.

bridging oxo ligands of *fully oxidize*d hexaniobate clusters feature the largest oxo-ligand electron densities observed for polyoxometalates, exceeding those of Mo and W clusters. Excitation of electrons to the Nb^V-based LUMO, to give Nb^{IV}, should *further enhance the already large electron density and nucleophilic* character of the bridging oxo atoms of Nb-μ_2-O-Nb linkages of the hexaniobate ligands, promoting effective coordination to the electrophilic carbon atom in CO_2.

Catalytic CO_2 reduction was investigated by placing an aqueous solution of **1** on a transparent window of fluorinated tin oxide (FTO), drying, insertion into 2.5 v:v % water: MeCN in a glass vessel under 1 atm CO_2, and irradiating with simulated solar light (Figure S16–S18). No sacrificial agents or photosensitizers were added. After 15 h, products in the headspace were analyzed by gas chromatography.

H_2 and CO were obtained at 86 % selectivity for CO at a rate per mass of NiO (core), much larger than that observed for 20 nm cubic-NiO NCs (Figure 5A). Per total mass of **1**, irradiation-intensity normalized rates of 17.8 and 108.2 $\mu mol\,g^{-1}\,h^{-1}$ of H_2 and CO, respectively, *exceed those of other catalysts reported to use solar-light and water to reduce CO_2 to H_2 and CO* (Table S6).

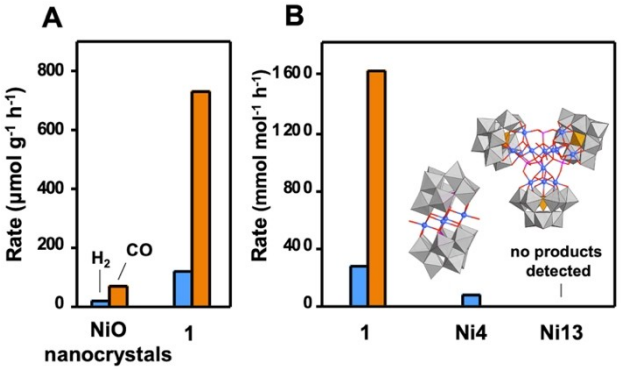

Figure 5. Photocatalytic reduction of CO_2 by H_2O under simulated solar light (150 W) with an intensity of 697 $mW\,cm^{-2}$. A) CO_2-reduction rates per mass of NiO for optimally-thin films of 20-nm cubic-NiO NCs and **1**. B) CO_2-reduction rates (molar basis) for films of **1** and molecular nickel-cluster photocatalysts, (**Ni4**)[16] and (**Ni13**),[26] shown using blue for Ni, red for O, orange for P, and grey for W-centered polyhedral.

Compared to Ni-based polyoxometalate photocatalysts: the H_2-evolution catalyst, $Na_{25}[Ni_{13}(H_2O)_3(OH)_9(PO_4)_4(SiW_9O_{34})_3]$ (**Ni13**),[26] was inactive, and $K_6Na_4[Ni_4(H_2O)_2(PW_9O_{34})_2]$ (**Ni4**),[16] showed little activity (Figure 5B and S19, S20). For NiO NCs, **1** and **Ni4**, no soluble organic products were detected by ^1H NMR analysis of MeCN reaction solutions (Figure S21).

Compared with 730 $\mu mol\,g^{-1}\,h^{-1}$ of CO produced under 1 atm CO_2 (Figure 5A and S22A), reaction under *air* (4×10^{-4} atm CO_2) gave no detectable products. One atm 99 atom-% $^{13}CO_2$ (Figure S23), gave only ^{13}CO, proving CO formation from CO_2.

Upon reduction of the water content from 2.5 to 0.08 v:v %, no products were observed, and with 98 atom-% $H_2{}^{18}O$ (2.5 v:v water), $^{18}O_2$ alone was found (Figure S24–25). Stoichiometric oxidative equivalents of O_2 were produced during seven repeat catalysis runs, during which *no decrease in activity was observed* (Figure S26, S27); no changes were observed in FTIR or powder-XRD spectra of **1** (Figure S28, S29).

DFT calculations, Figure 6, addressed coordination of CO_2 and water to **1** (panel A) and conversion of CO_2 to CO (panel B). At the outset of photoexcitation, water is bound to Ni centers (left in Figure 6A; $-5.2\,kcal\,mol^{-1}$), while upon photogeneration of Nb^{IV}, the highly electron dense oxo atoms of Nb^{IV}-μ_2-O-Nb^V linkages are sufficiently nucleophilic to bind CO_2 (right in Figure 6A; $-20.7\,kcal\,mol^{-1}$). Subsequent reduction of a second Nb atom to Nb^{IV} is followed by the coupled transfer of two electrons and two H^+ to CO_2, from Nb^{IV} and water, respectively, to give bound CO, H-bonded H_2O and two equivalents of OH^- (Figure 6B). Determinations of full reaction mechanisms for water oxidation[27] and CO_2 reduction[28] by polyoxometalates are very complex and additional computational studies are currently underway.

In summary, soluble macroanions, **1**, feature 30 Ni^{II}-ion cubic-phase like $\{Ni_{30}O_{118}\}$ cores complexed by 10 hexaniobate, $[Nb_6O_{19}]^{8-}$, ligands. DFT calculations and in situ XPS

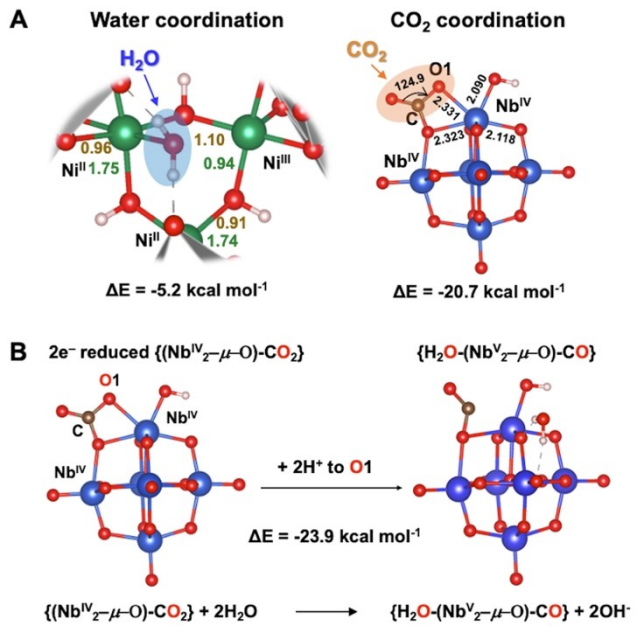

Figure 6. DFT calculated coordination and CO_2 reduction. A) Coordination of H_2O and CO_2 to photoexcited NiO and reduced hexaniobate. B) CO_2 reduction. Addition of two H^+ from water to O1 of bound CO_2 induces cleavage of the C–O1 bond, giving bound CO and H-bonded H_2O1 (at right).

show that solar-light promotes electrons from a Ni^{II} based conduction band of $\{Ni_{30}O_{118}\}$ to the Nb^V based LUMO of hexaniobate (Figure 4A) decreasing the energy needed to generate Nb^{IV} from 5 eV (typical of polyoxoniobate cluster-anions) to 3.6 eV, similar to pure and functionalized solid-state polyniobates. While photogenerated NiO "holes" oxidize water, reduction of Nb^V to Nb^{IV} increases the already large electron densities of bridging oxides of the hexaniobate ligands, rendering them sufficiently nucleophilic to bind CO_2, with protons from water triggering energetically favorable proton-coupled electron transfer to CO_2. More generally, the findings suggest that complexation of phase-defined fragments of visible-light semiconductors may provide a general method for transforming polyoxoniobate cluster-anions into photocatalysts for the solar-light driven binding and activation of small molecules.

Acknowledgements

I.A.W. thanks the Israel Science Foundation (280/21). G.Z. thanks PBC-Israel for a fellowship. J.M.P. thanks the Spanish Ministry of Science and Innovation (grant PID2020-112762GB-I00). This project has also received funding from the European Union's Horizon 2020 research and innovation program under the Marie Skłodowska-Curie grant agreement no. 713679 and from the Universitat Rovira i Virgili (URV).

Conflict of Interest

The authors declare no conflict of interest.

Data Availability Statement

The data that support the findings of this study are openly available in Cambridge Crystallographic Data Centre at http://www.ccdc.cam.ac.uk/data request/cif, reference number 2109911.

Keywords: CO_2 Reduction · Hexaniobate Anion · Molecular Complex · Nickel Oxide · Photocatalysis

[1] a) B. N. Nunes, O. F. Lopes, A. O. T. Patrocinio, D. W. Bahnemann, *Catalysts* **2020**, *10*, 126; b) C. Zhou, R. Shi, G. I. N. Waterhouse, T. Zhang, *Coord. Chem. Rev.* **2020**, *419*, 213399.
[2] a) B. N. Nunes, D. W. Bahnemann, A. O. T. Patrocinio, *ACS Appl. Energy Mater.* **2021**, *4*, 3681–3692; b) M. E. Strayer, J. M. Binz, M. Tanase, S. M. Kamali Shahri, R. Sharma, R. M. Rioux, T. E. Mallouk, *J. Am. Chem. Soc.* **2014**, *136*, 5687–5696.
[3] a) S. Nishioka, T. Oshima, S. Hirai, D. Saito, K. Hojo, T. E. Mallouk, K. Maeda, *ACS Catal.* **2021**, *11*, 659–669; b) W. Zhang, R. Uppuluri, T. E. Mallouk, C. T. Campbell, *J. Am. Chem. Soc.* **2020**, *142*, 15751–15763; c) T. Oshima, D. Lu, O. Ishitani, K. Maeda, *Angew. Chem. Int. Ed.* **2015**, *54*, 2698–2702; *Angew. Chem.* **2015**, *127*, 2736–2740; d) M. E. Strayer, T. P. Senftle, J. P. Winterstein, N. M. Vargas-Barbosa, R. Sharma, R. M. Rioux, M. J. Janik, T. E. Mallouk, *J. Am. Chem. Soc.* **2015**, *137*, 16216–16224.
[4] D. Y. Wan, Y. L. Zhao, Y. Cai, T. C. Asmara, Z. Huang, J. Q. Chen, J. Hong, S. M. Yin, C. T. Nelson, M. R. Motapothula, B. X. Yan, D. Xiang, X. Chi, H. Zheng, W. Chen, R. Xu, Ariando, A. Rusydi, A. M. Minor, M. B. H. Breese, M. Sherburne, M. Asta, Q.-H. Xu, T. Venkatesan, *Nat. Commun.* **2017**, *8*, 15070.
[5] S. Xie, Y. Wang, Q. Zhang, W. Deng, Y. Wang, *Chem. Commun.* **2015**, *51*, 3430–3433.
[6] R. Pang, K. Teramura, H. Asakura, S. Hosokawa, T. Tanaka, *Appl. Catal. B* **2017**, *218*, 770–778.
[7] a) G. Yin, M. Nishikawa, Y. Nosaka, N. Srinivasan, D. Atarashi, E. Sakai, M. Miyauchi, *ACS Nano* **2015**, *9*, 2111–2119; b) H. Hata, Y. Kobayashi, V. Bojan, W. J. Youngblood, T. E. Mallouk, *Nano Lett.* **2008**, *8*, 794–799.
[8] a) P. Huang, C. Qin, Z.-M. Su, Y. Xing, X.-L. Wang, K.-Z. Shao, Y.-Q. Lan, E.-B. Wang, *J. Am. Chem. Soc.* **2012**, *134*, 14004–14010; b) Z. Zhang, Q. Lin, D. Kurunthu, T. Wu, F. Zuo, S.-T. Zheng, C. J. Bardeen, X. Bu, P. Feng, *J. Am. Chem. Soc.* **2011**, *133*, 6934–6937.
[9] a) F. Steffler, R. L. A. Haiduke, *J. Mol. Struct.* **2021**, *1246*, 131156; b) D. J. Sures, P. I. Molina, P. Miró, L. N. Zakharov, M. Nyman, *New J. Chem.* **2016**, *40*, 928–936; c) G. J.-P. Deblonde, A. Moncomble, G. Cote, S. Bélair, A. Chagnes, *RSC Adv.* **2015**, *5*, 7619–7627.
[10] a) P. Mialane, C. Mellot-Draznieks, P. Gairola, M. Duguet, Y. Benseghir, O. Oms, A. Dolbecq, *Chem. Soc. Rev.* **2021**, *50*, 6152–6220; b) L. Chen, W.-L. Chen, X.-L. Wang, Y.-G. Li, Z.-M. Su, E.-B. Wang, *Chem. Soc. Rev.* **2019**, *48*, 260–284; c) S.-S. Wang, G.-Y. Yang, *Chem. Rev.* **2015**, *115*, 4893–4962; d) C. L. Hill, C. M. Prosser-McCartha, *Coord. Chem. Rev.* **1995**, *143*, 407–455.

[11] G. Zhang, M. Baranov, F. Wang, J. M. Poblet, S. Kozuch, N. Leffler, A. I. Shames, J. M. Clemente-Juan, A. Neyman, I. A. Weinstock, *J. Am. Chem. Soc.* **2021**, *143*, 20769–20778.
[12] M. Nyman, *Dalton Trans.* **2011**, *40*, 8049–8058.
[13] a) A. Misra, K. Kozma, C. Streb, M. Nyman, *Angew. Chem. Int. Ed.* **2020**, *59*, 596–612; *Angew. Chem.* **2020**, *132*, 606–623; b) S. S. Leiser, L. Polin, G. Gan-Or, M. Raula, I. A. Weinstock, *Inorg. Chem.* **2019**, *58*, 1012–1015; c) J.-H. Son, W. H. Casey, *Chem. Commun.* **2015**, *51*, 12744–12747.
[14] a) J. Niu, F. Li, J. Zhao, P. Ma, D. Zhang, B. Bassil, U. Kortz, J. Wang, *Chem. Eur. J.* **2014**, *20*, 9852–9857; b) Z. Liang, D. Zhang, P. Ma, J. Niu, J. Wang, *Chem. Eur. J.* **2015**, *21*, 8380–8383.
[15] a) M. Raula, G. Gan Or, M. Saganovich, O. Zeiri, Y. Wang, M. R. Chierotti, R. Gobetto, I. A. Weinstock, *Angew. Chem. Int. Ed.* **2015**, *54*, 12416–12421; *Angew. Chem.* **2015**, *127*, 12593–12598; b) B. Chakraborty, G. Gan-Or, M. Raula, E. Gadot, I. A. Weinstock, *Nat. Commun.* **2018**, *9*, 4896; c) B. Chakraborty, G. Gan-Or, Y. Duan, M. Raula, I. A. Weinstock, *Angew. Chem. Int. Ed.* **2019**, *58*, 6584–6589; *Angew. Chem.* **2019**, *131*, 6656–6661; d) Y. Duan, B. Chakraborty, C. K. Tiwari, M. Baranov, T. Tubul, N. Leffler, A. Neyman, I. A. Weinstock, *ACS Catal.* **2021**, *11*, 11385–11395; e) T. Tubul-Sterin, M. Baranov, G. Gan-Or, N. Leffler, A. Neyman, I. A. Weinstock, *Inorg. Chem.* **2022**, https://doi.org/10.1021/acs.inorgchem.1c03857.
[16] X.-B. Han, Y.-G. Li, Z.-M. Zhang, H.-Q. Tan, Y. Lu, E.-B. Wang, *J. Am. Chem. Soc.* **2015**, *137*, 5486–5493.
[17] a) J.-y. Tang, R.-t. Guo, W.-g. Zhou, C.-y. Huang, W.-g. Pan, *Appl. Catal. B* **2018**, *237*, 802–810; b) K. Nakaoka, J. Ueyama, K. Ogura, *J. Electroanal. Chem.* **2004**, *571*, 93–99.
[18] Deposition Number 2109911 contains the supplementary crystallographic data for this paper. These data are provided free of charge by the joint Cambridge Crystallographic Data Centre and Fachinformationszentrum Karlsruhe Access Structures service.
[19] W. L. Roth, *Phys. Rev.* **1958**, *110*, 1333–1341.
[20] a) M. A. Peck, M. A. Langell, *Chem. Mater.* **2012**, *24*, 4483–4490; b) M. M. Natile, A. Glisenti, *Chem. Mater.* **2002**, *14*, 4895–4903; c) A. N. Mansour, *Surf. Sci. Spectra* **1994**, *3*, 239–246.
[21] a) M. Rubinstein, R. H. Kodama, S. A. Makhlouf, *J. Magn. Magn. Mater.* **2001**, *234*, 289–293; b) B. Dong, W. Li, X. Huang, Z. Ali, T. Zhang, Z. Yang, Y. Hou, *Nano Energy* **2019**, *55*, 37–41.
[22] a) M. Ghosh, K. Biswas, A. Sundaresan, C. N. R. Rao, *J. Mater. Chem.* **2006**, *16*, 106–111; b) J. B. Yi, J. Ding, Y. P. Feng, G. W. Peng, G. M. Chow, Y. Kawazoe, B. H. Liu, J. H. Yin, S. Thongmee, *Phys. Rev. B* **2007**, *76*, 224402; c) M. Tadic, D. Nikolic, M. Panjan, G. R. Blake, *J. Alloys Compd.* **2015**, *647*, 1061–1068.
[23] a) R. Li, W. Zhang, K. Zhou, *Adv. Mater.* **2018**, *30*, 1705512; b) Y. Wang, X.-H. Liu, Q. Wang, M. Quick, S. A. Kovalenko, Q.-Y. Chen, N. Koch, N. Pinna, *Angew. Chem. Int. Ed.* **2020**, *59*, 7748–7754; *Angew. Chem.* **2020**, *132*, 7822–7828.
[24] A. Kudo, K. Sayama, A. Tanaka, K. Asakura, K. Domen, K. Maruya, T. Onishi, *J. Catal.* **1989**, *120*, 337–352.
[25] a) J. Choi, N. King, P. A. Maggard, *ACS Nano* **2013**, *7*, 1699–1708; b) K. Maeda, M. Eguchi, W. J. Youngblood, T. E. Mallouk, *Chem. Mater.* **2009**, *21*, 3611–3617.
[26] H. Lv, W. Guo, K. Wu, Z. Chen, J. Bacsa, D. G. Musaev, Y. V. Geletii, S. M. Lauinger, T. Lian, C. L. Hill, *J. Am. Chem. Soc.* **2014**, *136*, 14015–14018.
[27] a) J. Soriano-López, D. G. Musaev, C. L. Hill, J. R. Galán-Mascarós, J. J. Carbó, J. M. Poblet, *J. Catal.* **2017**, *350*, 56–63; b) K. Azmani, M. Besora, J. Soriano-López, M. Landolsi, A.-L. Teillout, P. de Oliveira, I.-M. Mbomekallé, J. M. Poblet, J.-R. Galán-Mascarós, *Chem. Sci.* **2021**, *12*, 8755–8766.
[28] a) C. Ci, J. J. Carbó, R. Neumann, C. D. Graaf, J. M. Poblet, *ACS Catal.* **2016**, *6*, 6422–6428; b) F. Wang, R. Neumann, C. de Graaf, J. M. Poblet, *ACS Catal.* **2021**, *11*, 1495–1504.

Manuscript received: September 6, 2022
Accepted manuscript online: October 6, 2022
Version of record online: November 4, 2022